International Journal of Biological Macromolecules 268 (2024) 131963

Contents lists available at ScienceDirect

International Journal of Biological Macromolecules

journal homepage: www.elsevier.com/locate/ijbiomac

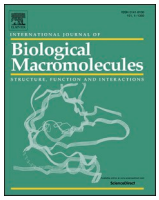

Designing an antimicrobial film for wound applications incorporating bacteriophages and ε-poly-L-lysine

Ana M. Pinto [a,b], Raquel Pereira [a], Artur J. Martins [a], Lorenzo M. Pastrana [a], Miguel A. Cerqueira [a], Sanna Sillankorva [a,*]

[a] INL – International Iberian Nanotechnology Laboratory, Av. Mestre José Veiga, 4715-330 Braga, Portugal
[b] CEB – Centre of Biological Engineering, LIBRO – Laboratório de Investigação em Biofilmes Rosário Oliveira, University of Minho, Campus de Gualtar, 4710-057 Braga, Portugal

ARTICLE INFO

Keywords:
Biodegradable
Sodium alginate
Gelatin
Active film
Wound healing
Bacteriophage

ABSTRACT

Alginate-based dressings have been shown to promote wound healing, leveraging the unique properties of alginate. This work aimed to develop and characterize flexible individual and bilayered films to deliver bacteriophages (phages) and ε-Poly-L-lysine (ε-PLL). Films varied in different properties. The moisture content, swelling and solubility increased with higher alginate concentrations. The water vapour permeability, crucial in biomedical films to balance moisture levels for effective wound healing, reached optimal levels in bilayer films, indicating these will be able to sustain an ideal moist environment. The bilayer films showed improved ductility (lower tensile strength and increased elongation at break) compared to individual films. The incorporated phages maintained viability for 12 weeks under vacuum and refrigerated conditions, and their release was sustained and gradual. Antibacterial immersion tests showed that films with phages and ε-PLL significantly inhibited *Pseudomonas aeruginosa* PAO1 growth (>3.1 Log CFU/cm^2). Particle release was influenced by the swelling degree and diffusional processes within the polymer network, providing insights into controlled release mechanisms for particles of varying size (50 nm to 6 μm) and charge. The films developed, demonstrated modulated release capabilities for active agents, and may show potential as controlled delivery systems for phages and wound healing adjuvants.

1. Introduction

Wound care is a critical biomedical subject that is difficult to master because it takes a long time for wounds to heal. Malnutrition, insufficient oxygen flow, smoking, diseases (such as diabetes and cancer), microbial infections, and other factors contribute to delayed wound healing [1,2]. *Acinetobacter baumannii*, *Klebsiella pneumoniae*, *Staphylococcus aureus*, and *Pseudomonas aeruginosa* are the most common wound-colonizing microorganisms that can cause significant tissue damage, and these microorganisms also induce septicemia, which raises the death rate from wound infections [3,4]. Moreover, many resistant bacteria are isolated from infected wounds, primarily because of the abuse and misuse of antibiotics. The fast interchange of genetic elements and resistance genes among bacterial classes promotes the spread of antimicrobial resistance [5].

Naturally occurring antimicrobials, such as phages, have been studied as potential antibiotic alternatives. Phages are highly specific against Gram-positive and Gram-negative bacteria and self-replicate, making them cost-effective [6]. Studies have demonstrated that phages can lyse multidrug-resistant (MDR) bacteria, suggesting that they might be used to prevent the propagation of these strains in the wound bed, preventing a more severe infection [7,8]. Furthermore, phages are harmless to humans and animals because they do not interact with other microbes [9]. Phages can be mixed to form "cocktails" to widen their host range, boost killing effectiveness, or prevent the development of phage resistance [10]. The inactivation of phages in physiological settings is one of the concerns for their free usage for medicinal therapies. When phages are exposed to serum antibodies, they can experience immune clearance and decrease phage infectivity [11]. Free phage administration is also undesirable and impracticable for deep tissue/organ infections [12]. Thus, phage inclusion in biomaterials may result in a prolonged local release of the phage load for higher efficacy. Another advantage of embedding phage in a biomaterial is that it allows it to be stored in off-the-shelf formulations [12].

* Corresponding author.
E-mail address: sanna.sillankorva@inl.int (S. Sillankorva).

https://doi.org/10.1016/j.ijbiomac.2024.131963
Received 17 October 2023; Received in revised form 5 April 2024; Accepted 27 April 2024
Available online 28 April 2024

Poly-L-lysine (PLL), a cationic polymer, has attracted significant attention in healthcare applications because of its biodegradability and biocompatibility [13]. PLL interacts with microbial membranes through rapid interactions with the hydrophobic core, surface interactions with phospholipid head-groups, and nonspecific membrane permeabilization *via* contact with positively and negatively charged groups [14–16]. Additionally, the composition of existing acyl chains in membranes influences PLL interaction [17]. For example, the interaction of PLL with membranes of *E. coli* and *L. innocua* involved PLL's binding to negatively charged phospholipids, resulting in the release of divalent cations and altering membrane curvature, potentially leading to the formation of vesicle-like structures [18]. This process ultimately caused cytoplasmic membrane permeabilization and destabilization. Among the PLL family, ε-Poly-L-lysine (ε-PLL) stands out as the most potent antibacterial agent, effectively impeding the proliferation of a wide array of microorganisms [19].

Selecting suitable materials for a particular wound is critical for successful healing. Natural polymer-based films have gained popularity in recent years due to their wide variety of applications, particularly in the pharmaceutical industry. Natural polysaccharides (*e.g.*, alginate, cellulose, chitin, and gelatin) are commonly used to develop bioactive materials due to their high biocompatibility, antibacterial activity, non-toxicity, and biodegradability.

Alginate is naturally present in brown seaweed and comprises blocks of (1,4)-linked β-D-mannuronate (M) and α-L-guluronate (G) at different ratios depending on the source [20]. The quantities and sequence of mannuronic and guluronic residues determine alginates' physical characteristics and molecular weight. Ionic crosslinking using divalent cations (*e.g.*, Ca^{2+}) can improve alginate films' forming strong, cohesive, non-adherent, and highly absorbent dressings permeable to oxygen and water vapour [21,22]. Furthermore, the calcium ions released into the wound help promote hemostasis by assisting in the clotting cascade, and the quantities of mannuronic and guluronic residues in the dressing determine the level of coagulation activation [23]. Because of the exceptional attributes of alginate, which encompass antimicrobial properties, non-toxic nature, high absorbency, non-allergic nature, breathability, hemostatic characteristics, and biocompatibility, its widespread utilization has been observed in the healing and regeneration of human tissue [24,25]. Previous studies have shown that the combination of alginate with gelatin results in biocompatible and biodegradable solutions that have interest, particularly for the production of wound dressings [26].

Gelatin is a natural polymer that may be made by hydrolyzing nonsoluble collagen. It comprises proline, glycine, and hydroxyproline and has an amino acid composition comparable to collagen, making it a natural mimic of the extracellular matrix (ECM) in human tissues and organs [1]. Also, gelatin includes peptide sequences that help cells recognize integrin receptors, which are essential for cell attachment [27]. Essentially, it tends to create nanofiber structures crucial for skin regeneration.

An ideal wound dressing should be an effective barrier against microbe penetration and have antimicrobial properties to prevent microbial growth beneath the dressing [28]. The current trend has focused on multilayer structures where the separation and release of drugs with different functions and at different times may be controlled, making the membranes more versatile [29]. Gelatin has been used to produce structures for wound care using layer-by-layer applications together with chitosan [30], polyvinyl alcohol [29], polyvinylpyrrolidone [31], among others. In addition, the combination of gelatin and alginate hydrogels [32–34], and fiber in films [35] has shown promising outcomes.

This work aimed to create a novel biodegradable and antimicrobial bilayer film made of sodium alginate and gelatin that includes phages as an antibiotic alternative for wound healing and an antimicrobial ε-PLL. Film characterization and film antimicrobial activity were assessed in this study, as well as phage release and stability. Our hypothesis suggests that the novel biodegradable bilayer film composed of sodium alginate and gelatin, incorporating phages and antimicrobial ε-PLL, will exhibit both effective antimicrobial properties and controlled phage release, making it a promising alternative for wound healing and infection management.

2. Materials and methodology

2.1. Materials

Gelatin from bovine skin Type B (CAS: 9000-70-8, ~225 g Bloom), alginic acid sodium salt (CAS: 9005-38-3; viscosity: 15–25 cP, 1 % in H_2O, 216.12 g/mol), and sodium chloride were acquired from Sigma-Aldrich (UK). Calcium chloride (CAS: 10043–52-4) was obtained from Supelco (Germany), and glycerol 99 % was obtained from Fisher Chemical (UK). Epolyly® (ε-Poly-L-lysine) was purchased from Handary (Belgium).

2.2. Bacteriophages

This work used *P. aeruginosa* PAO1 (DSM 22644). The *Pseudomonas* phages used were vB_PaeM_SMS21 (MN615701) and vB_PaeP_SPCB (MN615698), which have been previously isolated and characterized [36]. Tryptic soy broth (TSB) and tryptone soy agar (TSA) medium were used to grow the bacteria and propagate the phages.

2.3. Films preparation and assembly

Gelatin/alginate-based films were prepared by dissolving 2 to 4 g of gelatin and alginate in distilled water under agitation (350 rpm) at 40 °C for 1 h (Table 1). In addition, 1 % (*v*/v) of glycerol was added as a plasticizer. The two phages, suspended in SM buffer [5.8 g/L NaCl, 2 g/L $MgSO_4 \bullet 7H_2O$, and 50 mL/L of 50 mM Tris-HCl (pH 7.5)], were added at a final concentration of 1×10^{10} plaque forming units (PFU)/mL and homogenized under magnetic agitation to ensure even distribution on the films. Twenty grams of the mixture were weighed and poured into Petri dishes (Ø = 9 cm). After, the films were dried at 40 °C for 24 h, crosslinked with a 0.5 % (*w/v*) $CaCl_2$ solution (previously optimized, data not shown), redried at room temperature for 24 h, and kept in desiccators containing a saturated solution of $Mg(NO_3)_2 \bullet 6H_2O$ at 53 % relative humidity (RH) and 20 °C.

Gelatin-based films were prepared by dissolving 4 g of gelatin and adding 1 % (*v*/v) of glycerol. Phage suspensions were added and homogenized at the same concentrations used for the films to ensure an even distribution of the phages on the films. Also, ε-PLL was added to a final concentration of 0.1562 mg/mL. The films were dried at 40 °C for 24 h and kept in desiccators at 53 % RH and 20 °C.

To produce the gelatin/alginate/gelatin bilayer films, pre-made 4 % gelatin films were airbrushed (Dexter, 0.33 mm nozzle diameter, ref. 16982301) four times with 1 % (*w/v*) carboxymethylcellulose (CMC). Immediately after the last CMC passage, pre-made gelatin/alginate films using were placed and pressed to adhere the two films.

Table 1
Formulations of the different gelatin (G) and alginate (A) films.

		Gelatin/alginate film		Gelatin film
	Film	G- % (w/v)	A % (w/v)	G % (w/v)
Individual	$G_{1.5}A_{0.5}$	1.5	0.5	0
	$G_{1.5}A_{2.5}$	1.5	2.5	0
	G_2A_2	2	2	0
	$G_{2.5}A_{1.5}$	2.5	1.5	0
	G_4	0	0	4
Bilayer	$G_{1.5}A_{0.5}G_4$	1.5	0.5	4
	$G_{1.5}A_{2.5}G_4$	1.5	2.5	4
	$G_2A_2G_4$	2	2	4
	$G_{2.5}A_{1.5}G_4$	2.5	1.5	4

2.4. Film thickness

The film's appearance was recorded by a digital camera of Samsung Galaxy A53 (Samsung Electronics Co., Ltd., Suwon, South Korea). The thickness of the films was measured using a micrometer (Electronic outside micrometer; Schut Geometrical Metrology, Germany) at a 0.001-mm accuracy. Measurements were taken at nine different locations of each film sample (Ø = 9 cm), and the average values were used for tensile tests.

2.5. Film's moisture content, and water solubility

For these assays, films were cut into 4 cm^2 squares and stored in a desiccator at 53 % RH for 24 h. The moisture content (MC) was determined as the mass loss of the film samples after drying at 105 °C for 24 h.

$$MC\ (\%) = [(M_0 - M)/M_0] \times 100 \quad (1)$$

where M_0 corresponds to the initial mass of the film and M to the mass of the film after drying.

The water solubility (WS) was determined following the drying of samples at 105 °C in an oven for 24 h, placing them in beakers containing 5 mL of distilled water, and the beakers were shaken (150 rpm) at room temperature for 24 h.

$$WS\ (\%) = [(M_0 - M_{in})/M_0] \times 100 \quad (2)$$

where M_{in} is the mass of the insoluble pieces of the film after drying.

The remaining insolubilized pieces were collected, dried at 105 °C for 24 h, and weighed ($n = 3$). MC and WS were expressed in percentages following Eqs. (1) and (2).

To determine the swelling of the films (SW) (Eq. (3)), films (4 cm^2, stored in a desiccator at 53 % RH for 24 h at room temperature) were weighed and immersed in 50 mL of distilled water for 24 h at room temperature. Afterward, they were removed and dried with filter paper to remove excess water and weighed again.

$$SW\ (\%) = [(S1 - S0)/S0] \times 100 \quad (3)$$

where S_1 represents the weight of the film after immersion, and S_0 represents the initial weight of the film before immersion. All measurements were repeated in triplicate for each type of film.

2.6. Water vapour transmission rate

Water vapour transmission rate (WVTR) was determined using a gravimetric method at 23 °C according to the desiccant method (ASTM E96/E96M 2010). In brief, films were sealed in aluminum foil masks on the top of a 30 cm^2 open payne permeability cup (Elcometer 5100/2, Belgium) containing 20 mL of distilled water (relative humidity (RH) of 0 %). The cups were placed inside a desiccator with silica beads, and equipped with a fan to promote an air circulation and keep a constant driving force. The water permeated through the film and absorbed by the desiccant was determined from the weight loss of the permeation cell over the 7 days duration of assay. WVTR was determined from the slope of the weight loss × time (g/24 h) obtained by linear regression, and the sample area (m^2) in contact with the water vapour. The result is the average ± standard deviation of three replicates.

$$WVTR\ \left(g/m^2/24\ h\right) = slope/sample\ area \quad (4)$$

2.7. Mechanical properties of the films

The mechanical properties of the films were measured following the methodology described in ASTM D882-10 with some modifications and using AGX-10kN texture analyzer (Shimadzu, Japan) equipped with a 500 N load cell. The equipment was controlled using TRAPEZIUMX-*V* software. The samples were previously conditioned at room temperature and 53 % RH. Each film strip (20 mm × 70 mm) was clamped between claws with an initial distance of 100 mm. Force and deformation were analyzed during extension at 50 mm/min. Tensile strength (TS) and Young's modulus (YM) results were obtained in MPa, and elongation-at-break (EB) results in percentage, respectively. At least six strips of each film were measured.

2.8. Fourier-transform infrared spectroscopy (FTIR)

FTIR spectra of the films were recorded at 4 cm^{-1} spectral resolution on a FTIR spectrometer (Bruker FT-IR VERTEX 80/80v - Boston, USA) with an Attenuated Total Reflectance mode (ATR) under vacuum, with a platinum crystal accessory in the wavenumber range: 4000–400 cm^{-1}. An average of 32 scans was collected for each scan. Air (open beam) was used as background before each scan. Three replica spectra were collected for each sample.

2.9. Non-isothermal oscillatory rheometry

The rheological characterization was performed using an Anton Paar MCR 302e (Anton Paar, Graz, Austria) rheometer equipped with a stainless-steel flat-plate geometry (PP50) of 50 mm operating at a 1 mm gap. Non-isothermal ramps were executed between 20 and 50 °C for the gel-sol and sol-gel transition experiments. A constant rate of 2 °C/min with a fixed frequency of 1 Hz was applied. To observe the thermal transitions, the sample was first placed at 50 °C, and the variations in the slope of the storage and loss moduli were recorded as a function of temperature. The Rheocompass software was used to control the equipment and gather the data.

2.10. Scanning electron microscopy (SEM)

Scanning electron microscopy (SEM) was used to examine the surface and cross-sectional microstructures of the films. Dry samples were mounted on aluminum stubs using carbon adhesive tape and sputter-coated with gold (Leica EM ACE200) and observed under SEM (Quanta FEG 650, FEI, USA) using an accelerating voltage of 5 kV. For cross-section observation, the samples were previously fractured using liquid nitrogen.

2.11. In vitro antimicrobial activity of the films

The antimicrobial activity of the films was evaluated using the immersion method. In brief, a bacterial suspension of *P. aeruginosa* PAO1 adjusted to a final concentration of 1×10^6 colony forming units (CFU)/mL was prepared, and 1 mL was poured into a 24-well microtiter plate. Gelatin/alginate and bilayer films with and without phages and ε-PLL were tested. The plates were incubated at 37 °C (120 rpm). After 24 h, the samples were collected, and the number of cells was determined by plating serial dilutions performed. A 10 mM ammonium iron (II) sulfate solution was used for the films incorporating phages to disrupt the antibacterial action of phages. Three independent experiments were performed in duplicate.

2.12. Phage release from the films

The release of both phages (phage cocktail) simultaneously from the films was determined by placing 1 × 1 cm^2 squares films in 15 mL of SM buffer with constant stirring (100 rpm) at 35 °C. Samples (100 μL) were taken at different time points under sterile conditions, and the buffer volume was replenished at each sampling time. The samples were serially diluted and plated as described previously [37] in *P. aeruginosa* PAO1. Three independent experiments were performed in triplicate.

2.13. Fluoresbrite® YG Microspheres release from the films

Fluoresbrite® YG Microspheres (Polysciences Europe GmbH - Germany) at different sizes (0.05, 6, and 45 μm) were incorporated within the individual films, and a release experiment, performed as mentioned previously, was carried out at different time points. Fluorescence intensity was read under a microplate reader (BioTek Synergy H1) at excitation and emission spectra of 441 nm and 486 nm, respectively, and a gain of 100 was used.

2.14. Phage stability inside the bilayer films

After vacuum storage at 4 °C, the phage stability within the bilayer films was assessed at various time intervals. The titer of integrated phages in the films was evaluated by incubating samples with a diameter of 1 cm in 15 mL tubes containing 2 mL of SM buffer for 1 h at 35 °C with vigorous agitation (250 rpm). The number of active phage particles was determined by PFU enumeration.

2.15. Statistics

GraphPad Prism 8.2.1 was used to conduct the statistical analysis. The data were analyzed using a one-way and two-way analysis of variance (ANOVA), and all graphical statistics are represented as a mean with standard deviation. Results were considered significantly different at $p < 0.05$ (* $p < 0.05$, ** $p < 0.01$, *** $p < 0.001$, and **** $p < 0.0001$).

3. Results and discussion

This study focused on the development and characterization of films varying in the concentrations of alginate and gelatin, which were combined with a gelatin film. Gelatin and alginate were chosen due to their unique properties that make them well-suited for producing wound dressings. These materials contribute to a natural healing process, while their biodegradable nature aligns with the growing emphasis on environmental sustainability in modern wound care practices.

3.1. Film's visual appearance

The gelatin/alginate films were generally smooth (Fig. 1a–d)) and became less flexible and opaque when higher concentrations of alginate (A) were used. To the touch, gelatin films (G_4) were more flexible, smooth, and translucent than gelatin/alginate films (Fig. 1e).

3.2. Scanning electronic microscopy

SEM images of the cross-sections and surface of the microstructure of the films individually and the bilayer film are shown in Fig. 2. All films appeared to be continuous and non-porous matrix. No phase separation or visible fissures indicated that the crosslinking process in the gelatin/alginate films (*e.g.*, $G_{2.5}A_{1.5}$ in Fig. 2) did not generate any physical incompatibility inside the matrix. G_4 film demonstrated a stable and homogeneous internal structure, indicating that an organized matrix had developed in the inner layers. The bilayer films (*e.g.*, $G_{2.5}A_{1.5}G_4$ in Fig. 2) were homogenous, with the two layers clearly visible.

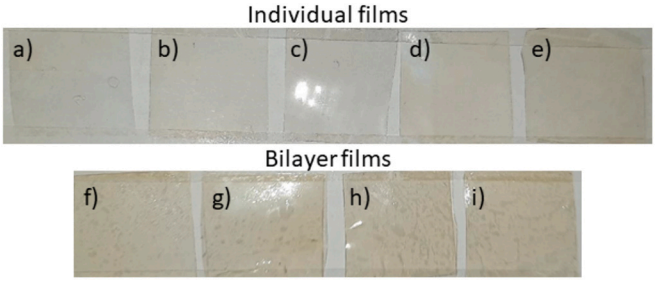

Fig. 1. The appearance of individual and bilayer films: a) $G_{1.5}A_{0.5}$; b) $G_{1.5}A_{2.5}$; c) G_2A_2; d) $G_{2.5}A_{1.5}$; e) G_4; f) $G_{1.5}A_{0.5}G_4$; g) $G_{1.5}A_{2.5}$ G_4; h) $G_2A_2G_4$; i) $G_{2.5}A_{1.5}G_4$.

Adding phages and ε-PLL did not cause morphological changes within the films compared to films devoid of phages (data not shown), indicating good compatibility. Previous studies using phages Listex P100 [9] and ϕIBB-PF7A [38] presented similar results. In bilayer films, adding CMC as an adhesive of the two films resulted in a visible separation of films.

3.3. Thickness

The thickness of individual and bilayer films is presented in Table 2. The G_4 films, consisting of 4 % of polymer mass, measured approximately 120 μm in thickness. Compared to these, the gelatin/alginate films, also with a total polymer mass of 4 % (G + A = 4 %) ($G_{1.5}A_{2.5}$ and G_2A_2) were less thick after drying. One plausible hypothesis is rooted in the application of CMC to a single side of a film. This action can potentially induce localized degradation or alterations in thickness within that specific film area.

Consequently, when the second film is introduced and pressed against the first, it may lead to irregularities in film thickness due to the influence of CMC. The crosslinking process with calcium chloride can also lead to differences in film thickness in dual-layered alginate and gelatin films compared to their individual counterparts. Alginate, known for its water-absorbing properties, tends to swell significantly when crosslinked with calcium ions, potentially leading to an increase in the thickness of the alginate layer [39]. Furthermore, interfacial interactions between the layers play a crucial role as calcium ions may diffuse into adjacent layers, influencing local properties and thickness at the interface. These combined effects of swelling and interfacial interactions result in differences in thickness between the dual-layered film and individual alginate and gelatin films.

Changes in gelatin concentration produced no discernible differences in most characteristics (*e.g.*, MC, S, and SW, data not shown) except for becoming thicker and less flexible. Since these latter two characteristics could delay phage release, only the 4 % gelatin concentration was used to produce bilayer films.

The thickness of the bilayer films varied between 164.11 μm ($G_2A_2G_4$) and 241.11 μm ($G_{1.5}A_{2.5}G_4$) and was higher than the sum of the thickness of each film individually. For instance, the $G_{1.5}A_{0.5}$ film had approximately 23.30 μm in thickness, and the G_4 film was 120 μm thick, and both combined should have an approximate theoretical thickness of 143.3 μm, which is lower than the 186.55 μm thickness measured. This might be related to a partial swelling phenomenon caused by adding CMC since the bilayer films were measured right after the adhesion process. Still, it may also be related to the thickness of the CMC used as an adhesive, as seen in Fig. 2, where the thin layer of CMC is clearly visible. Although visible, the SEM samples of the bilayer films were imaged fully dry; therefore, the possible swelling is not observed.

3.4. Moisture content and solubility

The water absorption properties of the films were analyzed by determining the moisture content and solubility (Table 2). The measurements revealed that the MC of films depended on the gelatin and alginate composition. Gelatin/alginate films with a lower ratio of gelatin to alginate showed higher MCs, possibly due to the interaction between hydrophilic groups in alginate and gelatin with water molecules. The MC was similarly found to decrease when the alginate concentration in the gelatin/alginate films dropped. On the other hand, the G_4 film had a higher MC than the gelatin/alginate films, which means that the incorporation of alginate has an important role in the film's MC. The MC values obtained for the bilayer films were close to the average value of the sum of the MC of the individual films.

The solubility is an important factor contributing to wound healing,

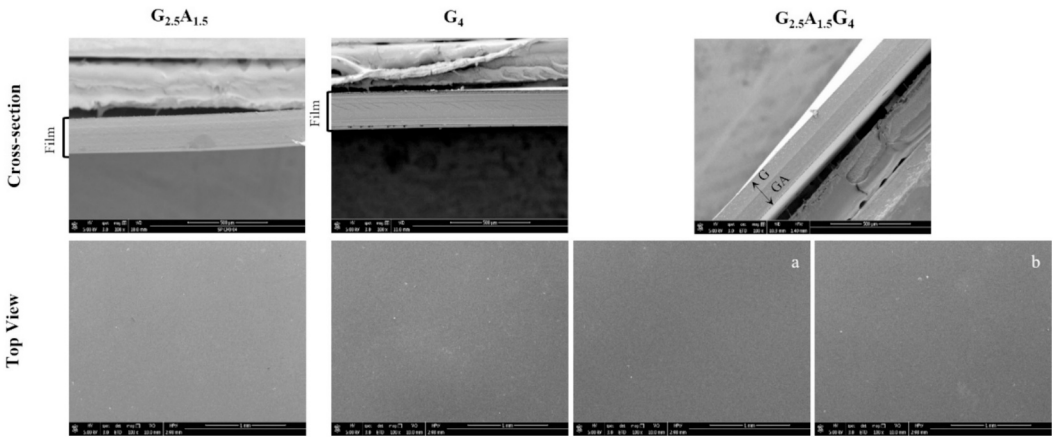

Fig. 2. SEM images of the cross-section and top view of the $G_{2.5}A_{1.5}$ and G_4 films imaged separately, and the respective $G_{2.5}A_{1.5}G_4$ bilayer film (on cross-section view, G corresponds to the gelatin film and GA to the gelatin/alginate film). Top view surfaces of the bilayer the $G_{2.5}A_{1.5}G_4$ film visualized from the two sides: a) $G_{2.5}A_{1.5}$ side and G_4 (b) side. Scale bar: 500 μm (cross-section) and 1 mm (top view).

Table 2
Values of thickness, moisture content (MC), solubility (S), and swelling index (SW) of the films.

	Film	Thickness (μm)	MC (%)	S (%)	SW (%)	WVTR (g/m^2/24 h)
Individual	$G_{1.5}A_{0.5}$	23.30 ± 2.90^a	21.12 ± 1.93^a	20.27 ± 2.93^a	236.48 ± 4.18^a	2851.16 ± 62.16^a
	$G_{1.5}A_{2.5}$	83.61 ± 1.33^b	12.44 ± 0.48^b	38.64 ± 1.77^b	909.92 ± 51.70^b	3008.33 ± 117.84 ^{a}
	G_2A_2	63.44 ± 7.07^b	11.77 ± 0.40^{bc}	28.19 ± 1.08^c	794.77 ± 48.18^b	3018.45 ± 283.20 ^{a}
	$G_{2.5}A_{1.5}$	69.94 ± 6.99^b	8.18 ± 0.43^{bc}	27.14 ± 0.42^c	564.03 ± 94.32^c	3084.54 ± 156.72 ^{a}
	G_4	120.00 ± 11.47^c	26.28 ± 0.27^d	35.27 ± 0.11^b	274.86 ± 11.82^a	3937.44 ± 238.56 ^{b}
Bilayer	$G_{1.5}A_{0.5}G_4$	186.55 ± 16.13^a	22.15 ± 3.54^a	31.53 ± 0.73^a	305.94 ± 12.26^a	2408.27 ± 268.32 ^{a}
	$G_{1.5}A_{2.5}G_4$	241.11 ± 13.44^b	18.34 ± 0.83^{ab}	34.58 ± 0.80^a	600.07 ± 54.34^b	1986.45 ± 200.40 ^{a}
	$G_2A_2G_4$	164.11 ± 26.66^a	17.34 ± 0.25^b	29.03 ± 1.56^{ab}	573.75 ± 33.62^b	2100.05 ± 336.24 ^{a}
	$G_{2.5}A_{1.5}G_4$	228.00 ± 19.16^b	17.16 ± 1.07^b	29.79 ± 0.86^{ab}	357.95 ± 52.72^a	1981.61 ± 127.44 ^{a}

All values reported correspond to the mean ± sd. Different superscripts a–d within the same column and major rows indicate significant differences ($p < 0.05$) among the values of a parameter between different films according to the analysis of variance (ANOVA).

and which will reduce pain during film removal. The solubility observed in this study is attributed to the hydrophilic characteristics of both gelatin and alginate. The solubility of gelatin/alginate films increased when the alginate concentrations were higher, except for $G_{1.5}A_{0.5}G_4$ bilayer film. The solubility *v*alues obtained for bilayers were nearly the average of the stand-alone gelatin/alginate and the gelatin films' solubility once the bilayers are constituted by half of each film [40]. Gelatin presents a high solubility in water, and adding alginate led to solubilities varying between 20 and 38 %. The solubility of 4 % (*w/v*) gelatin - 3 % (w/v) alginate gels, which were 60 μm thick, was reported to be close to 47 % [41], while the WS of 2 % (w/v) gelatin - 2 % (w/v) alginate gels was found to be around 65 % [42]. However, there is no reference to the thickness of the films produced in the latter study. It is difficult to compare our results with other published literature as the film properties, including solubility, are not only polymer mass but also thickness and production method dependent [43].

3.5. Swelling degree

The gelatin/alginate ratio influenced the swelling of the rehydrated dry films when in contact with water (Table 2). Overall, the swelling was higher in films having a higher alginate content. The rise in the swelling ratio may be credited to an increase in hydrophilic groups of films [44]. In addition, the physical entanglement of alginate's and gelatin's polymeric chains contributes to the creation of a network known to have an increased swelling index [44]. Also, the films with a higher swelling presented an increased solubility. For instance, the $G_{1.5}A_{2.5}$ films presented a swelling index of approximately 909.92 % and solubility of 34.58 %, while the $G_{1.5}A_{0.5}$ films swelled the least, resulting in a solubility of 20.27 %.

The crosslinking process explains the gelatin/alginate films' good swelling ability and stability since the gelatin blocks the link to the calcium ions, forming an "egg-box" conformation. This feature increases the film's resistance while lowering its swelling capacity when applying high divalent ion concentrations.

The G_4 film was not crosslinked, implying that the SW achieved (274.86 %) was solely due to the film's intrinsic tendency to swell.

Regarding the bilayer films, adding the G_4 film to the individual films caused a decrease in SW compared to each gelatin/alginate film individually. Since the two films are glued to each other, this might result in a lower contact area of the gelatin/alginate films with water. Therefore, we can hypothesize that half of each gelatin/alginate and gelatin film's sum is expressed in the final bilayer films. However, the area of each film that swelled was impossible to estimate.

The swelling characteristics obtained are ideal for the absorption of wound secretions, will protect the wounds from getting wet and will help in promoting healing.

3.6. Water vapour transmission rate (WVTR)

The water vapour permeability, generally quantified by water vapour transmission rate (WVTR), assesses the ability to regulate water evaporation and maintain hydration equilibrium on either side of a biomedical film [45]. Many parameters can influence this parameter including density, pore structure, surface chemistry, crystallinity, and the parameters chosen for film drying [46].

WVTR in porous membranes is prompted by vapour concentration gradients, facilitating the flow of water vapour through membrane channels from regions of high RH to those of lower RH [47]. Some wounds need moisture removal, others need existing moisture retained

in the dressing, and some require added moisture. The main challenge is to strike a balance when selecting a dressing that can manage exudate effectively at different stages of wound healing. Too much or too little moisture, as controlled by the WVTR of the dressing, can impact the wound healing process negatively. Commercially available wound dressings, typically have WVTR values in the range from 100 to 3300 g/m^2/24 h [48]. Queen et al. have proposed that a WVTR ranging from 2000 to 2500 g/m^2/24 h would maintain sufficient moisture levels without the potential for desiccation [49]. Furthermore, *in vitro* and *in vivo* studies have proved that a WVTR of 2030 g/m^2/24 h was optimal for sustaining an ideal moist environment for cells, both within cultured settings and in a murine model simulating full-thickness wound healing [50]. Hasatsri et al. tested 6 different (two hydrocolloids, two alginates, and two foam) wound dressings and their results showed that the hydrocolloid dressings did not possess proper water vapour permeation conditions, and the best WVTR were observed with calcium sodium alginate dressings, which also demonstrated the highest absorbent qualities [51]. In another study, microporous polyurethane membrane dressings were developed possessing different WVTR values [50]. The authors concluded that WVTR was the main factor affecting wound healing, as all different membranes showed similar oxygen permeation abilities. A WVTR of 2028 g/m^2/24 h maintained optimal moisture for the proliferation and functions of epidermal cells and fibroblasts in a 3D culture models, and the *in vivo* tests revealed proliferation and migration of these cells through up regulation of the expression of α-smooth muscle actin and proliferating cell nuclear antigen, and downregulation of the expression of E-cadherin. In our studies (Table 2), individual films presented WVTR values above 2800 g/m^2/24 h. These values are beyond the defined optimal range. It seems that films with higher gelatin content tend to have higher WVTR values, supported by the trend of increasing WVTR values as the weight percentage of gelatin increases from G1.5 (2851.16 g/m^2/24 h) to G4 (>3900 g/m^2/24 h). Although the WVTR values in individual films were above the optimal range, merging the individual films with the G4 films, to create the bilayer films, decreased the WVTR values to values very comparable to those suggested as optimal for maintaining an ideal environment. This decrease in WVTR was likely caused by a reduction in the porosity of the bilayer films, which slowed down gas diffusion.

3.7. Mechanical properties

The values of the tensile strength (TS), elongation-at-break (EB), and Young's modulus (YM) were evaluated for the characterization of films and bilayer films' intensity, extensibility, and rigidity, respectively (Table 3). These are essential parameters for fabricating wound dressings and characterizing their strength and flexibility. Whether applied topically to prevent cutaneous wounds or used as interior wound support, a wound dressing should be flexible, malleable, and not prone to rip or rupture when applied [2,52].

The gelatin/alginate films produced were quite stiff, broke nearly immediately at the start of the test, and displayed brittle and inflexible material features. The typical stress-strain curves of both individual (Fig. S1a) and bilayer (Fig. S1b) films exhibit a characteristic profile of a tough material without a yield point with a linear elasticity leading to fracture. This means that all the observed deformation (non-elastic) is permanent for both sets of samples. The tensile strength of individual films reaches higher values; however, bilayer films can be strained slightly more when compared to the individual films, indicating that the addition of the gelatin (G) to film composition contributes to an increased level of flexibility in the bilayer structure. For instance, they presented a high YM and TS at the expense of a lower EB, which meets the findings of Dong et al. [53]. The maximum TS values were achieved using a higher concentration of alginate (and a corresponding reduction in gelatin). This might be owing to the occurrence of polymer-polymer intermolecular interactions.

Contrarily, the G_4 film has far lower YM values than the gelatin/alginate films, implying that they are significantly more flexible and break later.

Combining the gelatin/alginate films with the G_4 films to create the bilayer film decreased the TS and increased the EB values compared to the gelatin/alginate films alone. Thus, including the G_4 film improved the ductility of the bilayer film. However, the overall extensibility of the bilayer film is close to that observed with gelatin/alginate films. During the analysis, it was also possible to observe that the gelatin/alginate films broke first while the G_4 films remained intact. Because of the G_4 film's flexibility, the gelatin/alginate films could hold their shape for extended periods, validating the results presented here.

3.8. Fourier-transform infrared spectroscopy (FTIR)

The FTIR analysis aimed to detect the presence of new chemical bonds or the alteration of existing ones mainly attributed to the presence of phages and/or the ε-PLL. FTIR spectra of pure gelatin, alginate, and ε-PLL are shown in Fig. 3, as well as the spectra of individual and bilayer films. In the pure alginate sample, two distinct absorption bands were found, at 1595 cm^{-1} and around 1402 cm^{-1}, attributable to the asymmetric and symmetric stretching vibration of the C—O bond of the —COO group, respectively. The peak at 1022 cm^{-1} corresponds to the antisymmetric stretch of C—O—C, and the peak at 806 cm^{-1} is typical of mannuronic acid residues [53].

Amide *I* (C═O and C—N stretching vibration), Amide II (mainly N—H bending vibration and C—N stretching vibration), and Amide III (mainly N—H bending vibration and C—N stretching vibration) were found to be responsible for the characteristic absorption bands of gelatin at 1629 cm^{-1}, 1523 cm^{-1}, and 1230 cm^{-1}, respectively [23]. Finally, Amide A, represented by the stretching vibration of O—H bonded to N—H, is characterized by a broad absorption band of approximately 3271 cm^{-1} [53,54]. Amide *B* is represented by the C—H stretching, and the —NH_2 stretching is characterized by a peak at 2937 cm^{-1}.

A very broad absorbance is visible in the 3300–2800 cm^{-1} and bands between 1700 and 1400 cm^{-1} in the ε-PLL spectra. The band at 1658 cm^{-1} corresponds to amide I, and the band at 1558 cm^{-1} correspond to

Table 3
Tensile strength (TS), elongation-at-break (EB), and Young's modulus (YM) of films.

	Film	EB (%)	TS (MPa)	YM (MPa)
Individual	$G_{1.5}A_{0.5}$	4.41 ± 1.61[a]	118.26 ± 36.68[a]	4443.92 ± 878.59[a]
	$G_{1.5}A_{2.5}$	8.10 ± 5.16[a]	71.01 ± 20.39[b]	2947.08 ± 1311.44[b]
	G_2A_2	6.12 ± 1.15[a]	85.13 ± 9.54[b]	2755.11 ± 624.21[b]
	$G_{2.5}A_{1.5}$	6.51 ± 1.89[a]	76.72 ± 8.32[b]	2244.34 ± 536.81[b]
	G_4	164.81 ± 41.23[b]	2.28 ± 0.42[c]	2.59 ± 0.91[c]
Bilayer	$G_{1.5}A_{0.5}G_4$	8.28 ± 3.68[a]	10.18 ± 3.48[a]	280.27 ± 116.04[a]
	$G_{1.5}A_{2.5}G_4$	13.56 ± 4.26[a]	13.92 ± 2.09[a]	416.20 ± 95.82[a]
	$G_2A_2G_4$	15.74 ± 11.64[a]	10.89 ± 2.28[a]	223.18 ± 49.89[a]
	$G_{2.5}A_{1.5}G_4$	10.74 ± 3.62[a]	16.59 ± 2.24[a]	485.21 ± 69.05[a]

Values reported are the mean ± SD, $n = 7$. Different superscripts a–c within the same column and major rows indicate significant differences among the values of a parameter between different films according to the analysis of variance (ANOVA).

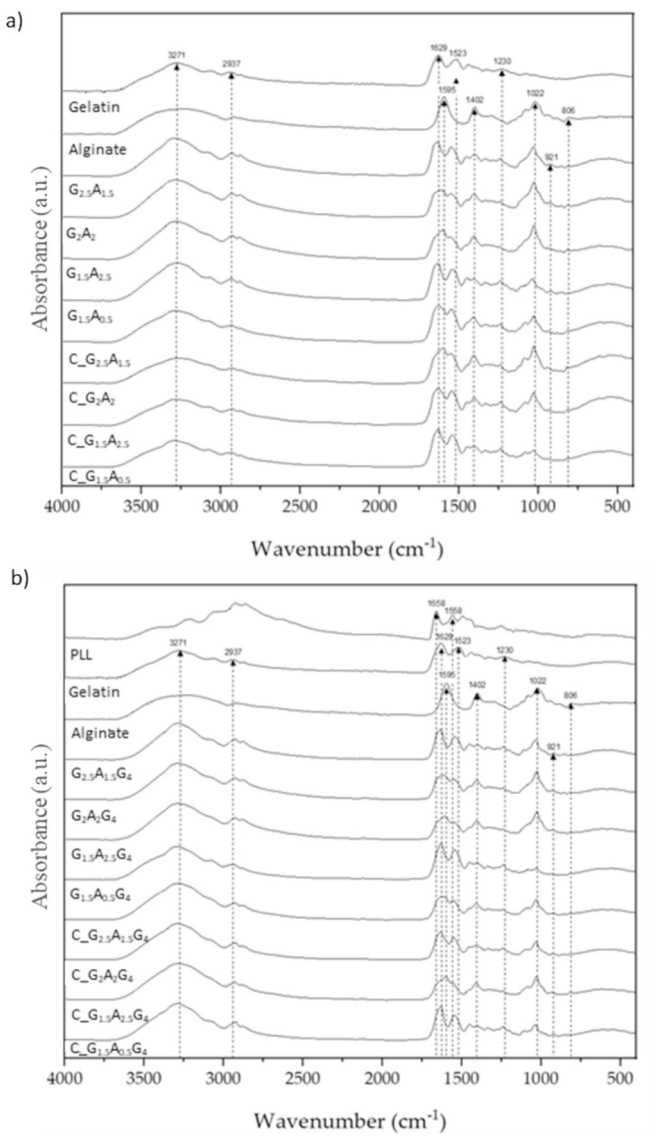

Fig. 3. FTIR spectra of the films compared to pure gelatin, alginate, and ε-PLL. a) Individual and b) bilayer films C_ refers to control samples without phages and ε-PLL (*e.g.*, C_ $G_{1.5}A_{0.5}$ refers to the $G_{1.5}A_{0.5}$ film without phages and ε-PLL). a.u. refer to arbitrary units.

amide II. Both correspond to the peptide group's vibrational modes [55,56]. Also, the typical C—O stretching band of glycerol was slightly accentuated between 930 and 900 cm^{-1} in the gelatin/alginate and the bilayer films [57].

No substantial changes were observed between the individual gelatin/alginate films and the bilayer films, with or without phages and ε-PLL. All films were analyzed with the gelatin layer side facing the crystal. There is in both the gelatin/alginate film and the bilayer films a broad band between 3000 and 3600 cm^{-1} attributable to the hydroxyl group stretching from alginate and N—H stretching of secondary amide from gelatin, as well as bands around 2930 and 2870 cm^{-1} for asymmetric and symmetric stretching modes of CH_2 and CH, respectively [9].

3.9. Non-isothermal oscillatory rheometry

Fig. S2 displays the results of temperature sweeps conducted under oscillatory conditions at a constant strain to measure the storage and loss moduli (*G'* and *G"*, respectively) of a 4 % (*w/v*) gelatin solution. These analyses elucidate the structural changes within the bilayer film formation, particularly gelatin, which was not crosslinked and, therefore, is in its natural form, diluted only in water.

The point where the storage modulus (*G'*) and the loss modulus (*G"*) curves intersect was used to determine the sol-gel transition temperature. The ramps for cooling and heating were carried out at the same speed. The viscoelastic moduli quickly rise as the temperature approaches 23 °C while cooling. The process is reversed in the heating ramp, and the viscoelastic moduli drop as the temperature rises (33 °C to liquid form). The process's thermoreversibility is supported by the observation that *G'* and *G"* arrive at the same starting point at 50 °C. However, a hysteresis occurs because the transition temperatures in the heating and cooling ramps differ.

Due to the gelatin random coils' great chain mobility at high temperatures, the rheological reaction behaves like a liquid-like system under these conditions. The gelation begins when the temperature drops and a three-dimensional network develops [58]. The initial production of the triple helices and their growth in number density is marked by an onset temperature, which is determined by the temperature at which the moduli increase abruptly [59]. When the gelation is finished, a solid-like behavior with an elastic modulus is noticeably more remarkable than the viscous one at low temperatures. At this point, the microstructure comprises a tightly coupled triple gelatin helices network.

The imposed rate determines the hysteresis produced between the heating and cooling ramps, narrowing as the ramp rate drops. The existence of a distinct energy barrier required to dissolve (during melting) and form (while cooling) the triple helices between gelatin chains has previously been used to justify this hysteresis [60]. In addition, gelatin gels are known to be non-equilibrium systems because of the continual development and rearranging of the helices amount over a long time scale, even if it is fair to predict that for an "infinitely low" ramp rate, the heating and cooling ramp might overlap [58,61,62].

Results provided insight into the similar phage release patterns observed across all tested films, as the release experiments were carried out at 35 °C. This temperature facilitated rapid liquefaction of the gelatin, the non-crosslinked component of the films, leading to the phages being released equally in all films, irrespective of their gelatin-to-alginate ratio.

3.10. In vitro antimicrobial activity of the films

The antimicrobial activity of the gelatin/alginate and bilayer films was tested using the immersion method (Fig. 4).

The immersion tests showed that *P. aeruginosa* PAO1 grew on the control films (films without phages and ε-PLL), reaching above 9.5 Log CFU/cm^2. In contrast, the growth of *P. aeruginosa* PAO1 was considerably inhibited in the presence of the gelatin/alginate and bilayer films incorporated with phages and ε-PLL, which presented statistical significance ($p < 0.05$) compared to the control films. All films containing phages and ε-PLL together decreased the number of viable bacteria by >3.1 Log CFU/cm^2. Incorporating phages into individual and bilayer films resulted in an effective antibacterial action (~99.9 %). All films were prepared with the same initial phage concentration (1×10^{10} PFU/mL). We can postulate that the minor differences may be related to their distribution within the film.

3.11. Phage release from the films

Evaluating the phage release profile is an important aspect that can impact the phage's efficacy. It is crucial to ensure that the phages are appropriately released so that they may act against the host bacteria colonizing the wound bed. Fig. 5 shows the phages' release profile from the films.

During the film manufacturing process, two phages were incorporated into the films casted onto Petri dishes (Ø 9 cm). Although two phages were used to decrease the emergence of resistant phenotypes, as previously shown [36], only the total concentration of phages released

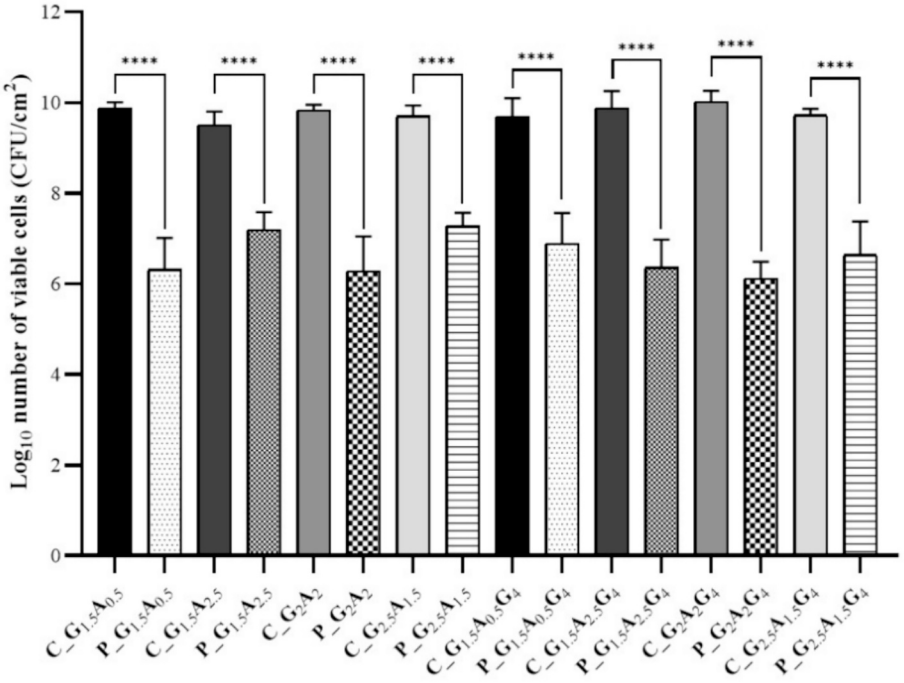

Fig. 4. Antimicrobial activity of the individual and bilayer films against *P. aeruginosa* PAO1 after 24 h of contact. C_ - control, P_ - with phages and ε-PLL. **** indicates significant differences ($p < 0.0001$) between control films and phage-entrapped in individual and bilayer films.

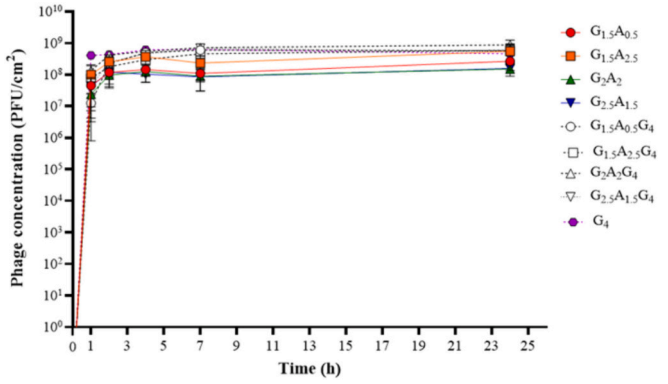

Fig. 5. *In vitro* release of the phage cocktail profile from each different individual and bilayer films at 35 °C at a pH = 7.5. Colored symbols and lines represent the individual films, while empty symbols show the release profile from bilayer films.

was determined. In theory, each 1 cm × 1 cm individual film used for the release studies consisted of approximately of 3.2×10^8 PFU/cm^2 (1.6×10^8 PFU/cm^2/phage), while the bilayer films (individual gelatin/alginate films joined to the gelatin film) presented about 6.4×10^8 PFU/cm^2. The number of phages released from individual films was within the expected range [1.51×10^8 (G_2A_2) up to 5.47×10^8 ($G_{1.5}A_{2.5}$) PFU/cm^2 ± standard deviation]. The number of phages released after 24 h from the bilayer films varied between 5.32×10^8 (G2.5:A1.5:G4) and 8.73×10^8 PFU/cm^2 (G2:A2:G4) and was higher than the expected values. Therefore, according to the results obtained (Fig. 5), it can be concluded that the release of phages was entirely accomplished within the study's timeframe. This release was gradual since the start of the experiment, indicating that neither the gelatin nor the alginate polymers affected, as expected, the phage lytic activity, causing insignificant phage losses. In individual films, phages were more rapidly released from the gelatin film, which was not crosslinked with $CaCl_2$, and from the films showing the highest alginate mass ($G_{1.5}A_{2.5}$) with the highest swelling index. Given the differences observed in each film characterization, particularly the swelling feature, it was expected that significant differences would be observed in the release profile. However, the effect of swelling in the release of phages was not fully clear since varying results were obtained with high and low swelling indices. For instance, there were minimal differences between the release profiles of the different films in bilayer films, which varied considerably in swelling index. Nonetheless, we observed that most phage load was discharged between 1 and 2 h of the swelling experiments. In a wound setting, however, phage release may not occur as smoothly as observed *in vitro* because, although the wound environment is moist, the films are not immersed in a liquid, resulting in a slower phage kinetic release.

3.12. *In vitro* release of Fluoresbrite® YG microspheres

To standardize the release profiles of individual gelatin (G) and gelatin/alginate films, we used Fluoresbrite® YG microspheres at three different sizes (50 nm, 6 μm, and 45 μm). The smallest particles were used to compare them with the release profiles obtained with bacteriophages SPCB and SMS21 (Fig. 6). The phages in question have approximate sizes of ~50 nm (SPCB) and 150 nm (SMS21), respectively [36].

Gelatin is known to have a high affinity for many types of fluorescent molecules. This high affinity can lead to increased retention of the microparticles in the gelatin matrix, resulting in higher fluorescence intensity. On the other hand, alginate is a linear polysaccharide that is negatively charged, and its interaction with fluorescent molecules largely depends on the molecule's size and properties.

The observed difference in fluorescence between the films with higher concentrations of gelatin and those with higher alginate concentrations may be attributed to these two polymers' chemical and physical properties and how they interact with the fluorescent microspheres used. According to this study, we can control the release kinetics depending on the particles' size. For instance, the smallest particles (0.05 μm) (Fig. 6C) were released similarly from all the different types of gel and faster than particles of 45 and 6 μm (Fig. 6A and B). These particles were steadily released during the initial 7 h, resulting in 80 %

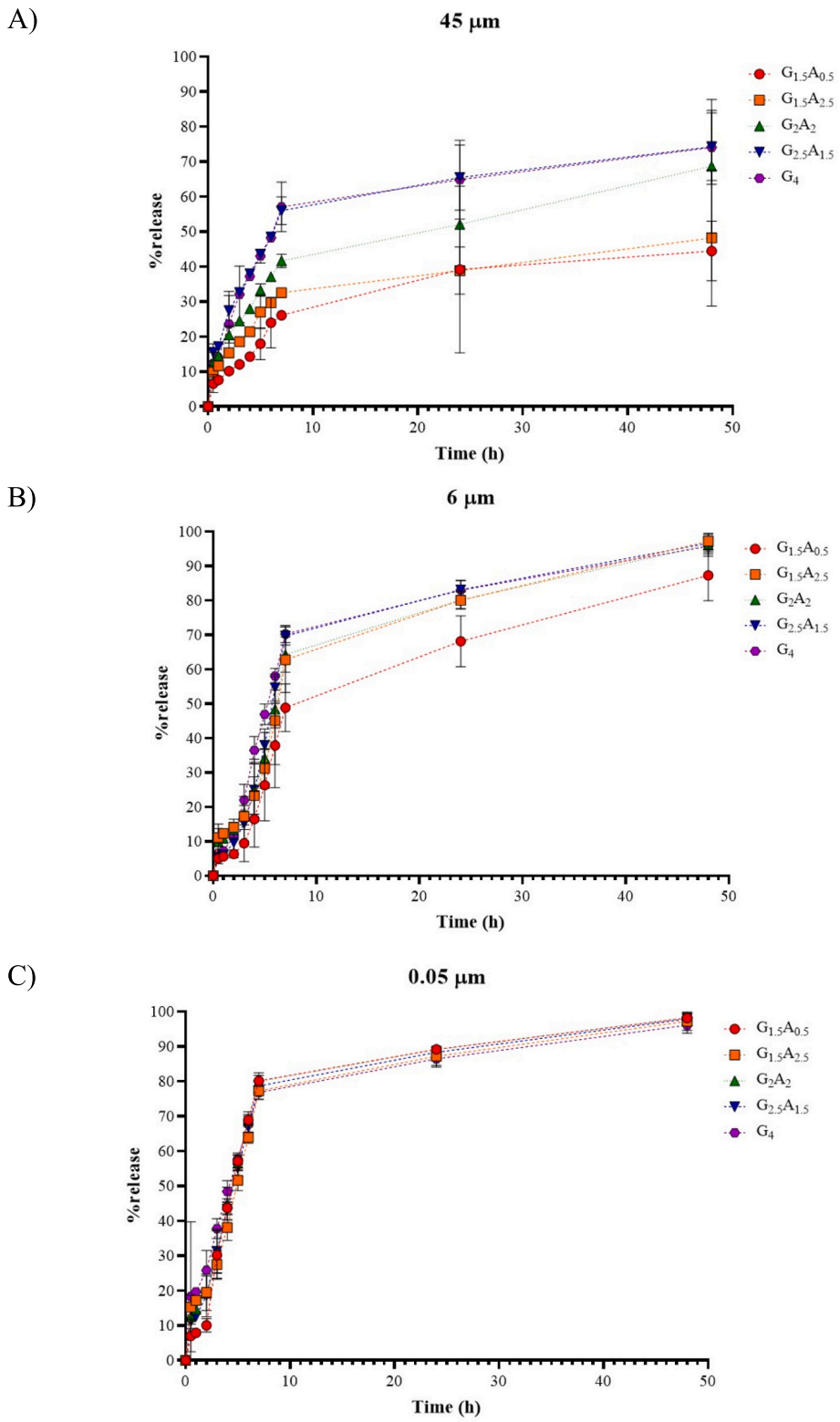

Fig. 6. *In vitro* release of Fluoresbrite® YG Microspheres of different sizes incorporated within the different individual films. Release of microspheres with a diameter of A) 45 µm; B) 6 µm; C) 0.05 µm from the individual films.

of particles released. This release was slower than the release obtained with phages, which are approximately the same size. Phages are known to adsorb better to hydrophobic matrices. Alginate and gelatin are both hydrophilic, and we hypothesize that phages were more rapidly released for this reason. These hydrophilic matrices have a greater affinity for water, and their structure may allow for easier and faster diffusion of phages into the surrounding aqueous environment. On the other hand, the fluorescent spheres used were hydrophobic polystyrene-based microspheres; therefore, they will be more retained in the hydrophilic alginate-gelatin films due to their water-repelling interaction.

The particles with the largest size were 30 to 60 % released in 7 h, and even in the last time point assessed (50 h), only 40 to 70 % had been

released (Fig. 6A). Similarly, particles of 6 μm (Fig. 6B) were 50–70 % released after 7 h, and 90 % released after 50 min. The release of these 45 μm and 6 μm (Fig. 6A and B) microspheres was negatively affected by the swelling degree of the films. Films with the highest swelling index considerably delayed the release of microspheres. High swelling can be advantageous for drug release, but it may also form a gel-like barrier restricting particle diffusion. This has been previously observed in rapidly swellable hydrogels [63,64], hydrophilic polymers and super-absorbent materials [65,66], where a gel-like structure is created, hindering the release of the drug. The film $G_{1.5}A_{0.5}$ was not considered in this comparison since the polymer mass was lower and the thickness was not comparable.

This work shows that the release of fluorescent microparticles from the films is affected by the mass and swelling of the polymers, depends on the sphere size, and is ruled by diffusional processes within the polymer network. Controlled release of other molecules varying in size and charge has been reported (see [67] for a more detailed review).

A lower mass of polymer can lead to less structural integrity of the film, which could cause a slower release of the microparticles. In addition, these films may have smaller pore sizes, which could further slowdown the release of the microparticles. The film $G_{2.5}A_{1.5}$ provides the optimal condition for microparticles to interact with the polymers.

The release kinetics also varied with differing thicknesses. For instance, in the case of the largest microparticles (45 μm), the release was slower in thicker films ($G_{1.5}A_{2.5}$), despite their higher swelling ratios, than in thinner films with lower swelling ratios. This phenomenon can be attributed to the distance the microparticles need to navigate through the film to be released. In thicker films, a longer path length may be required for the microparticles to diffuse out, which can lead to slower release rates. Conversely, thinner films may have a shorter distance for the particles to travel, resulting in a relatively faster release rate. These findings suggest that the interplay between film thickness and microparticle size can play a critical role in modulating drug release kinetics, which may have implications for the design of drug delivery systems.

Also, crosslinking the gelatin/alginate films with a $CaCl_2$ solution creates a more stable network of polymer chains within the film. This can result in smaller pores and a more uniform structure, slowing down the release of the microparticles from the film. Additionally, the ionic interactions between Ca^{2+} ions and the negatively charged alginate chains can lead to stronger crosslinking, further decreasing the release rate. On the other hand, if the concentration of $CaCl_2$ used for crosslinking is too high, it could cause excessive crosslinking of the polymer chains, leading to a very tight network with very small or no pores. This could ultimately hinder the release of microparticles from the film. In our study, we used a $CaCl_2$ solution with a concentration of 0.5 %. This concentration is relatively low compared to higher crosslinking concentrations, such as 1 % or 2 % $CaCl_2$ solutions. Thus, based on the results obtained in our experiment, it appears that the concentration of $CaCl_2$ solution utilized is not the primary factor responsible for any observed differences in microparticle release rates between the various films tested.

3.13. Phage stability inside the bilayer films

Phage stability inside the bilayer films was assessed over 12 weeks (Fig. 7).

The testing of bilayer films was specifically chosen to evaluate the full potential of both layers in maintaining phage stability. Furthermore, the inner gelatin layer can provide a barrier effect to prevent phages from migrating to the outer alginate layer, where they may be more susceptible to environmental stresses. In addition, the alginate layer can provide additional protection by acting as a buffer against pH changes and other external factors.

The results show no significant decreases in phage activity after 12 weeks. These results meet the expectations since several studies reported

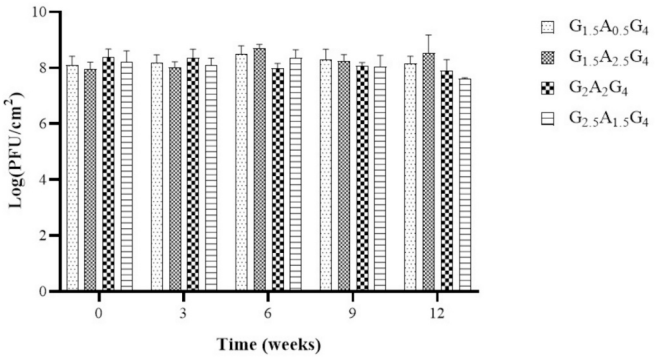

Fig. 7. Stability of phages in bilayer films under vacuum and refrigerated conditions (4 °C) during 12 weeks.

that biopolymers such as alginate confer good phage stability under low temperatures and protection from harsh conditions such as the ones encountered in the intestine [68,69].

Given that an initial concentration of 1×10^{10} PFU/mL was added to the film solutions, an average log decrease of 1.75 was observed after production (0 weeks). This decrease may be caused by drying the films at 40 °C for 24 h and the temperature used to prepare the gelatin and alginate solutions [70]. Besides this titer decrease, the bacteriophages retained their viability and lytic activity in the bilayer films after the gelatin/alginate film crosslinking with Ca^{2+} ions. It has already been stated that the crosslinking process does not affect the phage titer. Contrarily, it has been shown that Ca^{2+} ions may, in fact, aid plaque development because they make it easier for phages to adhere to bacterial receptors [71]. Divalent ions promote the spread of bacteriophages up to a point, but at very high concentrations, they inhibit the spread of phages [72].

4. Conclusions

In our study, we successfully developed and characterized bio-based and bioactive individual and bilayer films for delivering active agents to wound sites. The primary focus of the study was to assess if phages and ε-PLL successfully incorporated into the films, retained their antimicrobial activity against *P. aeruginosa*, a common wound pathogen. We explored different gelatin-to-alginate ratios to formulate the films, which can modulate the release of active ingredients such as phages, which typically have a nanoscale size. We also used microparticles with larger sizes (6 and 45 μm), to mimic other additional molecules that can be used in skin regeneration and wound healing applications. In addition, the film-immobilized bacteriophages maintained their lytic activity at least for three months, and were released to kill *P. aeruginosa*. In addition, we performed different studies to characterize the film properties. In general, the bilayer films produced displayed enhanced ductility compared to individual film configurations, optimal water vapour permeability, and are made of materials with good biodegradability and biocompatibility. This suggests that these films can potentially be used as a delivery system for bacteriophages and other wound healing adjuvants, enabling localized and controlled antimicrobial distribution over an extended period. Further research is needed to determine water resistance, oxygen permeation due to oxygen's role in cellular metabolism and tissue repair processes, and enzymatic degradation to confirm that the dressing developed maintains structural integrity and resists breakdown by enzymes in the wound environment (*e.g.*, proteases and collagenases) over time. Also, it is important to define the optimal quantity of bacteriophages for therapeutic effects, potentially through *in vitro* and *ex vivo* biofilm models. Unlike traditional dressings, these films offer antimicrobial activity, and advantageous material properties for promoting wound healing.

CRediT authorship contribution statement

Ana M. Pinto: Writing – original draft, Methodology, Investigation, Formal analysis. **Raquel Pereira:** Investigation, Formal analysis. **Artur J. Martins:** Writing – original draft, Methodology, Investigation, Formal analysis. **Lorenzo M. Pastrana:** Writing – review & editing, Supervision, Funding acquisition, Conceptualization. **Miguel A. Cerqueira:** Writing – review & editing, Supervision, Funding acquisition, Formal analysis, Conceptualization. **Sanna Sillankorva:** Writing – review & editing, Validation, Supervision, Project administration, Funding acquisition, Formal analysis, Conceptualization.

Declaration of competing interest

The authors declare that they have no known competing financial interests or personal relationships that could have appeared to influence the work reported in this paper.

Acknowledgments

This study was supported by the Portuguese Foundation for Science and Technology (FCT) under the scope of the strategic funding of UID/BIO/04469/2020 unit. A.M.P. acknowledges FCT for the grants SFRH/BD/138138/2018 and COVID/BD/152935/2022. S.S. acknowledges funding by FCT through the individual scientific employment program contract (2020.03171.CEECIND).

Appendix A. Supplementary data

Supplementary data to this article can be found online at https://doi.org/10.1016/j.ijbiomac.2024.131963.

References

[1] S.P. Ndlovu, K. Ngece, S. Alven, B.A. Aderibigbe, Gelatin-based hybrid scaffolds: promising wound dressings, Polymers (Basel). 13 (2021), https://doi.org/10.3390/polym13172959.
[2] E. Rezvani Ghomi, S. Khalili, S. Nouri Khorasani, R. Esmaeely Neisiany, S. Ramakrishna, Wound dressings: current advances and future directions, J. Appl. Polym. Sci. 136 (2019) 47738, https://doi.org/10.1002/app.47738.
[3] S. Esposito, G. De Simone, Update on the main MDR pathogens: prevalence and treatment options, Infez. Med. 25 (2017) 301–310.
[4] World Health Organization, Antimicrobial resistance. (2018). https://www.who.int/news-room/fact-sheets/detail/antimicrobial-resistance (accessed January 8, 2023).
[5] B. Loh, V.S. Gondil, P. Manohar, F.M. Khan, H. Yang, S. Leptihn, Encapsulation and delivery of therapeutic phages, Appl. Environ. Microbiol. 87 (2020) e01979-20, https://doi.org/10.1128/aem.01979-20.
[6] F. Nogueira, N. Karumidze, I. Kusradze, M. Goderdzishvili, P. Teixeira, I. C. Gouveia, Immobilization of bacteriophage in wound-dressing nanostructure, nanomedicine nanotechnology, Biol. Med. 13 (2017) 2475–2484, https://doi.org/10.1016/j.nano.2017.08.008.
[7] A.M. Pinto, M.A. Cerqueira, M. Bañobre-Lópes, L.M. Pastrana, S. Sillankorva, Bacteriophages for chronic wound treatment: from traditional to novel delivery systems, Viruses 12 (2020) 235, https://doi.org/10.3390/v12020235.
[8] L.D.R. Melo, H. Oliveira, D.P. Pires, K. Dabrowska, J. Azeredo, Phage therapy efficacy: a review of the last 10 years of preclinical studies, Crit. Rev. Microbiol. 46 (2020) 78–99, https://doi.org/10.1080/1040841X.2020.1729695.
[9] C.L. de Dicastillo, L. Settier-Ramírez, R. Gavara, P. Hernández-Muñoz, G. L. Carballo, Development of biodegradable films loaded with phages with antilisterial properties, Polymers (Basel). 13 (2021) 1–15, https://doi.org/10.3390/polym13030327.
[10] Y. Yang, W. Shen, Q. Zhong, Q. Chen, X. He, J.L. Baker, K. Xiong, X. Jin, J. Wang, F. Hu, S. Le, Development of a bacteriophage cocktail to constrain the emergence of phage-resistant *Pseudomonas aeruginosa*, Front. Microbiol. 11 (2020) 327, https://doi.org/10.3389/fmicb.2020.00327.
[11] K. Dąbrowska, Phage therapy: what factors shape phage pharmacokinetics and bioavailability? Systematic and critical review, Med. Res. Rev. 39 (2019) 2000–2025, https://doi.org/10.1002/med.21572.
[12] S.G. Rotman, E. Sumrall, R. Ziadlou, D.W. Grijpma, R.G. Richards, D. Eglin, T. F. Moriarty, Local bacteriophage delivery for treatment and prevention of bacterial infections, Front. Microbiol. 11 (2020) 2276, https://doi.org/10.3389/fmicb.2020.538060.
[13] P. Zarrintaj, S. Ghorbani, M. Barani, N.P. Singh Chauhan, M. Khodadadi Yazdi, M. R. Saeb, J.D. Ramsey, M.R. Hamblin, M. Mozafari, E. Mostafavi, Polylysine for skin regeneration: a review of recent advances and future perspectives, Bioeng, Transl. Med. 7 (2022), https://doi.org/10.1002/btm2.10261.
[14] M.N. Melo, R. Ferre, M.A.R.B. Castanho, Antimicrobial peptides: linking partition, activity and high membrane-bound concentrations, Nat. Rev. Microbiol. 7 (2009) 245–250, https://doi.org/10.1038/nrmicro2095.
[15] E. Glukhov, M. Stark, L.L. Burrows, C.M. Deber, Basis for selectivity of cationic antimicrobial peptides for bacterial versus mammalian membranes, J. Biol. Chem. 280 (2005) 33960–33967, https://doi.org/10.1074/jbc.M507042200.
[16] D. Sengupta, H. Leontiadou, A.E. Mark, S.J. Marrink, Toroidal pores formed by antimicrobial peptides show significant disorder, Biochim. Biophys. Acta Biomembr. 1778 (2008) 2308–2317, https://doi.org/10.1016/j.bbamem.2008.06.007.
[17] B.S. Vad, K. Bertelsen, C.H. Johansen, J.M. Pedersen, T. Skrydstrup, N.C. Nielsen, D.E. Otzen, Pardaxin permeabilizes vesicles more efficiently by pore formation than by disruption, Biophys. J. 98 (2010) 576–585, https://doi.org/10.1016/j.bpj.2009.08.063.
[18] M. Hyldgaard, T. Mygind, B.S. Vad, M. Stenvang, D.E. Otzen, R.L. Meyer, The antimicrobial mechanism of action of epsilon-poly-L-lysine, Appl. Environ. Microbiol. 80 (2014) 7758–7770, https://doi.org/10.1128/AEM.02204-14.
[19] E. Lebaudy, C. Guilbaud-Chéreau, B. Frisch, N.E. Vrana, P. Lavalle, The high potential of ε-poly-l-lysine for the development of antimicrobial biomaterials, Adv. NanoBiomed Res. 3 (2023), https://doi.org/10.1002/anbr.202300080.
[20] D. Lee, Mooney, alginate: properties and biomedical applications, Prog. Polym. Sci. 37 (2012) 106–126, https://doi.org/10.1016/j.progpolymsci.2011.06.003.
[21] A. Sood, M.S. Granick, N.L. Tomaselli, Wound dressings and comparative effectiveness data, Adv. Wound Care 3 (2014) 511–529, https://doi.org/10.1089/wound.2012.0401.
[22] M.J. Costa, A.M. Marques, L.M. Pastrana, J.A. Teixeira, S.M. Sillankorva, M. A. Cerqueira, Physicochemical properties of alginate-based films: effect of ionic crosslinking and mannuronic and guluronic acid ratio, Food Hydrocoll. 81 (2018) 442–448, https://doi.org/10.1016/j.foodhyd.2018.03.014.
[23] H.C. Segal, B.J. Hunt, K. Gilding, The effects of alginate and non-alginate wound dressings on blood coagulation and platelet activation, J. Biomater. Appl. 12 (1998) 249–257, https://doi.org/10.1177/088532829801200305.
[24] S. Tavakoli, A.S. Klar, Advanced hydrogels as wound dressings, Biomolecules 10 (2020) 1–20, https://doi.org/10.3390/biom10081169.
[25] R. Raus, W. Nawawi, R. Nasaruddin, Alginate and alginate composites for biomedical applications, Asian, J. Pharm. Sci. 16 (2021) 280–306, https://doi.org/10.1016/j.ajps.2020.10.001.
[26] B. Sarker, D.G. Papageorgiou, R. Silva, T. Zehnder, F. Gul-E-Noor, M. Bertmer, J. Kaschta, K. Chrissafis, R. Detsch, A.R. Boccaccini, Fabrication of alginate-gelatin crosslinked hydrogel microcapsules and evaluation of the microstructure and physico-chemical properties, J. Mater. Chem. B 2 (2014) 1470–1482, https://doi.org/10.1039/c3tb21509a.
[27] R. Naomi, H. Bahari, P.M. Ridzuan, F. Othman, Natural-based biomaterial for skin wound healing (gelatin vs. collagen): expert review, Polymers 13 (2021), https://doi.org/10.3390/polym13142319.
[28] O. Sarheed, A. Ahmed, D. Shouqair, J. Boateng, Antimicrobial dressings for improving wound healing, Wound Heal. - New Insights into Anc. Challenges. (2016) 373–398. doi:https://doi.org/10.5772/63961.
[29] S.-M. Huang, S.-M. Liu, H.-Y. Tseng, W.-C. Chen, Development and *in vitro* analysis of layer-by-layer assembled membranes for potential wound dressing: electrospun curcumin/gelatin as middle layer and gentamicin/polyvinyl alcohol as outer layers, Membranes (Basel). 13 (2023) 564, https://doi.org/10.3390/membranes13060564.
[30] W. Zheng, C. Chen, X. Zhang, X. Wen, Y. Xiao, L. Li, Q. Xu, F. Fu, H. Diao, X. Liu, Layer-by-layer coating of carboxymethyl chitosan-gelatin-alginate on cotton gauze for hemostasis and wound healing, Surf. Coatings Technol. 406 (2021), https://doi.org/10.1016/j.surfcoat.2020.126644.
[31] H.D. López-Calderón, H. Avilés-Arnaut, L.J. Galán Wong, V. Almaguer-Cantú, J. R. Laguna-Camacho, C. Calderón-Ramón, J.E. Escalante-Martínez, K. Arévalo-Niño, Electrospun polyvinylpyrrolidone-gelatin and cellulose acetate bi-layer scaffold loaded with gentamicin as possible wound dressing, Polymers (Basel). 12 (2020) 1–12.
[32] F. Cadamuro, V. Ardenti, F. Nicotra, L. Russo, Alginate–gelatin self-healing hydrogel produced via static–dynamic crosslinking, Molecules 28 (2023) 1–13, https://doi.org/10.3390/molecules28062851.
[33] F. Fayyazbakhsh, M.J. Khayat, M.C. Leu, 3D-printed gelatin-alginate hydrogel dressings for burn wound healing: a comprehensive study, Int. J. Bioprinting. 8 (2022) 274–291, https://doi.org/10.18063/ijb.v8i4.618.
[34] N.G. Kim, S.C. Kim, T.H. Kim, J.Y. Je, B. Lee, S.G. Lee, Y.M. Kim, H.W. Kang, Z. J. Qian, N. Kim, W.K. Jung, Ishophloroglucin a-based multifunctional oxidized alginate/gelatin hydrogel for accelerating wound healing, Int. J. Biol. Macromol. 245 (2023) 125484, https://doi.org/10.1016/j.ijbiomac.2023.125484.
[35] A. Sharma, V. Puri, P. Kumar, I. Singh, Rifampicin-loaded alginate-gelatin fibers incorporated within transdermal films as a fiber-in-film system for wound healing applications, Membranes (Basel). 11 (2021) 1–16, https://doi.org/10.3390/membranes11010007.
[36] A.M. Pinto, A. Faustino, L.M. Pastrana, M. Bañobre-López, S. Sillankorva, *Pseudomonas aeruginosa* PAO1 *in vitro* time–kill kinetics using single phages and phage formulations—modulating death, adaptation, and resistance, Antibiotics 10 (2021) 877, https://doi.org/10.3390/antibiotics10070877.
[37] M.D. Adams, Bacteriophages, Interscience Publishers, New York, 1959.
[38] D. Alves, M.J. Costa, S.M. Sillankorva, A. Marques, M.A. Cerqueira, C. Milho, L. M. Pastrana, Bacteriophage ϕIBB-PF7A loaded on sodium alginate-based films to

prevent microbial meat spoilage, Int. J. Food Microbiol. 291 (2018) 121–127, https://doi.org/10.1016/j.ijfoodmicro.2018.11.026.
[39] J.W. Rhim, Physical and mechanical properties of water resistant sodium alginate films, LWT 37 (2004) 323–330, https://doi.org/10.1016/j.lwt.2003.09.008.
[40] A.R.V. Ferreira, C.A.V. Torres, F. Freitas, C. Sevrin, C. Grandfils, M.A.M. Reis, V. D. Alves, I.M. Coelhoso, Development and characterization of bilayer films of FucoPol and chitosan, Carbohydr. Polym. 147 (2016) 8–15, https://doi.org/10.1016/j.carbpol.2016.03.089.
[41] R. Jafari, M. Zandi, A. Ganjloo, Characterization of alginate-gelatin edible film containing anise (<i>*Pimpinella anisum*<i/> L.) essential oil, J. Polym. Environ. 31 (2023) 1568–1583. doi:https://doi.org/10.1007/s10924-022-02707-8.
[42] H. Li, W. Li, J. Zhang, G. Xie, T. Xiong, H. Xu, Preparation and characterization of sodium alginate/gelatin/ag nanocomposite antibacterial film and its application in the preservation of tangerine, Food Packag. Shelf Life 33 (2022) 100928, https://doi.org/10.1016/j.fpsl.2022.100928.
[43] A.A. Tyuftin, J.P. Kerry, Gelatin films: study review of barrier properties and implications for future studies employing biopolymer films, Food Packag. Shelf Life 29 (2021) 100688, https://doi.org/10.1016/j.fpsl.2021.100688.
[44] N. Chiaoprakobkij, S. Seetabhawang, N. Sanchavanakit, M. Phisalaphong, Fabrication and characterization of novel bacterial cellulose/alginate/gelatin biocomposite film, J. Biomater. Sci. Polym. Ed. 30 (2019) 961–982, https://doi.org/10.1080/09205063.2019.1613292.
[45] X. Mi, H. Xu, Y. Yang, Submicron amino acid particles reinforced 100% keratin biomedical films with enhanced wet properties via interfacial strengthening, Colloids Surfaces B Biointerfaces. 177 (2019) 33–40, https://doi.org/10.1016/j.colsurfb.2019.01.043.
[46] S.S. Ahankari, A.R. Subhedar, S.S. Bhadauria, A. Dufresne, Nanocellulose in food packaging: a review, Carbohydr. Polym. 255 (2021) 117479, https://doi.org/10.1016/j.carbpol.2020.117479.
[47] S. Shi, Y. Si, Y. Han, T. Wu, M.I. Iqbal, B. Fei, R.K.Y. Li, J. Hu, J. Qu, Recent progress in protective membranes fabricated via electrospinning: advanced materials, biomimetic structures, and functional applications, Adv. Mater. 34 (2022) 2107938, https://doi.org/10.1002/adma.202107938.
[48] N. Ahmad, D. Tayyeb, I. Ali, N.K. Alruwaili, W. Ahmad, A. ur Rehman, A.H. Khan, M.S. Iqbal, Development and characterization of hemicellulose-based films for antibacterial wound-dressing application, Polymers (Basel). 12 (2020), https://doi.org/10.3390/polym12030548.
[49] D. Queen, J.D.S. Gaylor, J.H. Evans, J.M. Courtney, W.H. Reid, The preclinical evaluation of the water vapour transmission rate through burn wound dressings, Biomaterials 8 (1987) 367–371, https://doi.org/10.1016/0142-9612(87)90007-X.
[50] R. Xu, H. Xia, W. He, Z. Li, J. Zhao, B. Liu, Y. Wang, Q. Lei, Y. Kong, Y. Bai, Z. Yao, R. Yan, H. Li, R. Zhan, S. Yang, G. Luo, J. Wu, Controlled water vapor transmission rate promotes wound-healing via wound re-epithelialization and contraction enhancement, Sci. Rep. 6 (2016) 1–12, https://doi.org/10.1038/srep24596.
[51] S. Hasatsri, A. Pitiratanaworanat, S. Swangwit, C. Boochakul, C. Tragoonsupachai, Comparison of the morphological and physical properties of different absorbent wound dressings, Dermatol. Res. Pract. 2018 (2018), https://doi.org/10.1155/2018/9367034.
[52] C. Shi, C. Wang, H. Liu, Q. Li, R. Li, Y. Zhang, Y. Liu, Y. Shao, J. Wang, Selection of appropriate wound dressing for various wounds, Front. Bioeng. Biotechnol. 8 (2020) 182, https://doi.org/10.3389/fbioe.2020.00182.
[53] Z. Dong, Q. Wang, Y. Du, Alginate/gelatin blend films and their properties for drug controlled release, J. Memb. Sci. 280 (2006) 37–44, https://doi.org/10.1016/j.memsci.2006.01.002.
[54] L. Ma, H. Yang, M. Ma, X. Zhang, Y. Zhang, Mechanical and structural properties of rabbit skin gelatin films, Int. J. Food Prop. 21 (2018) 1203–1218, https://doi.org/10.1080/10942912.2018.1476874.
[55] M. Rozenberg, G. Shoham, FTIR spectra of solid poly-l-lysine in the stretching NH mode range, Biophys. Chem. 125 (2007) 166–171, https://doi.org/10.1016/j.bpc.2006.07.008.
[56] S. Maeda, Y. Fujiwara, C. Sasaki, K.K. Kunimoto, Structural analysis of microbial poly(ε-L-lysine)/poly(acrylic acid) complex by FT-IR, DSC, and solid-state 13C and 15N NMR, Polym. J. 44 (2012) 200–203, https://doi.org/10.1038/pj.2011.108.
[57] C. Peña-Rodriguez, J.F. Martucci, L.M. Neira, A. Arbelaiz, A. Eceiza, R. A. Ruseckaite, Functional properties and *in vitro* antioxidant and antibacterial effectiveness of pigskin gelatin films incorporated with hydrolysable chestnut tannin, Food Sci. Technol. Int. 21 (2015) 221–231, https://doi.org/10.1177/1082013214525429.
[58] M. Djabourov, J.P. Lechaire, F. Gaill, Structure and rheology of gelatin and collagen gels, Biorheology (1993) 191–205, https://doi.org/10.3233/BIR-1993-303-405.
[59] L. Guo, R.H. Colby, C.P. Lusignan, T.H. Whitesides, Kinetics of triple helix formation in semidilute gelatin solutions, Macromolecules 36 (2003) 9999–10008, https://doi.org/10.1021/ma034264s.
[60] C. Michon, G. Cuvelier, B. Launay, Concentration dependence of the critical viscoelastic properties of gelatin at the gel point, Rheol. Acta. 32 (1993) 94–103, https://doi.org/10.1007/BF00396681.
[61] V. Normand, S. Muller, J.C. Ravey, A. Parker, Gelation kinetics of gelatin: a master curve and network modeling, Macromolecules 33 (2000) 1063–1071, https://doi.org/10.1021/ma9909455.
[62] S.B. Ross-Murphy, Incipient behaviour of gelatin gels, Rheol. Acta 30 (1991) 401–411, https://doi.org/10.1007/BF00396526.
[63] J. Siepmann, F. Siepmann, Swelling controlled drug delivery systems, in: M. Siepmann, J., Siegel, R., Rathbone (Ed.), Fundam. Appl. Control. Release Drug Deliv., Springer, 2012: pp. 153–170. doi:https://doi.org/10.1007/978-1-4614-0881-9.
[64] W. Zhang, P. Wang, S. Liu, J. Chen, R. Chen, X. He, G. Ma, Z. Lei, Factors affecting the properties of superabsorbent polymer hydrogels and methods to improve their performance: a review, J. Mater. Sci. 56 (2021) 16223–16242, https://doi.org/10.1007/s10853-021-06306-1.
[65] P. Ghasemiyeh, S. Mohammadi-Samani, Polymers blending as release modulating tool in drug delivery, Front. Mater. 8 (2021) 1–12, https://doi.org/10.3389/fmats.2021.752813.
[66] M.S. Paolini, O.S. Fenton, J.L. Bhattacharya, Chandrabali Andresen, R. Langer, Polymers for extended-release administration, Biomed. Microdevices 21 (2019).
[67] W.R. Gombotz, S.F. Wee, Protein release from alginate matrices, Adv. Drug Deliv. Rev. 31 (1998) 267–285, https://doi.org/10.1016/S0169-409X(97)00124-5.
[68] E. Gonzalez-Menendez, L. Fernandez, D. Gutierrez, A. Rodríguez, B. Martínez, P. GarcíaI, Comparative analysis of different preservation techniques for the storage of *Staphylococcus* phages aimed for the industrial development of phage-based antimicrobial products, PloS One 13 (2018) 1–14, https://doi.org/10.1371/journal.pone.0205728.
[69] A.S. Abdelsattar, F. Abdelrahman, A. Dawoud, I.F. Connerton, A. El-Shibiny, Encapsulation of *E. Coli* phage ZCEC5 in chitosan–alginate beads as a delivery system in phage therapy, AMB Express (2019), https://doi.org/10.1186/s13568-019-0810-9.
[70] L. Stipniece, D. Rezevska, J. Kroica, K. Racenis, Effect of the biopolymer carrier on *Staphylococcus aureus* bacteriophage lytic activity, Biomolecules 12 (2022), https://doi.org/10.3390/biom12121875.
[71] P. Serwer, S.J. Hayes, S. Zaman, K. Lieman, M. Rolando, S.C. Hardies, Improved isolation of undersampled bacteriophages: finding of distant terminase genes, Virology 329 (2004) 412–424, https://doi.org/10.1016/j.virol.2004.08.021.
[72] M.I. Qadir, Z. Chauhdary, Antibacterial activity of novel strains of bacteriophages: an experimental approach, Crit. Rev. Eukaryot. Gene Expr. 28 (2018) 1–12, https://doi.org/10.1615/CritRevEukaryotGeneExpr.2017019608.